An Insight into the Mechanism of Inhibition and Reactivation of the F_1-ATPases by Tentoxin†

Jérôme Santolini,‡,§ Claire Minoletti,‡,¶ Jean-Marie Gomis,$ Claude Sigalat,‡,# François André,‡,# and Francis Haraux*,‡,#

Service de Bioénergétique, DBJC, CEA Saclay, 91191 Gif-sur-Yvette Cedex, France, Protéines Membranaires Transductrices d'Énergie, CNRS URA 2096, CEA Saclay, 91191 Gif-sur-Yvette Cedex, France, and Service des Molécules Marquées, DBJC, CEA Saclay, 91191 Gif-sur-Yvette Cedex, France

Received November 13, 2001; Revised Manuscript Received March 1, 2002

ABSTRACT: The mechanism of inhibition and reactivation of chloroplast ATP-synthase by the fungal cyclotetrapeptide tentoxin was investigated by photolabeling experiments, binding studies, and kinetic analysis using synthetic analogues of tentoxin. The α-subunit of chloroplast F_1-ATPase (CF_1) was specifically labeled by a photoactivatable tentoxin derivative, providing the first direct evidence of tentoxin binding to the α-subunit, and 3D homology modeling was used to locate tentoxin in its putative binding site at the α/*β* interface. The nonphotosynthetic F_1-ATPase from thermophilic bacterium (TF_1) proved to be also tentoxin-sensitive, and enzyme turnover dramatically increased the rate of tentoxin binding to its inhibitory site, contrary to what was previously observed with ϵ-depleted CF_1 [Santolini, J., Haraux, F., Sigalat, C., Moal, G., and André, F. (1999) *J. Biol. Chem. 274*, 849−858]. We propose that tentoxin preferentially binds to an ADP-loaded α*β* pair, and mechanically blocks the catalytic cycle, perhaps by the impossibility of converting this α*β* pair into an ATP-loaded α*β* pair. Using ^{14}C-tentoxin and selected synthetic analogues, we found that toxin binding to the tight inhibitory site of CF_1 exerts some cooperative effect on the loose reactivatory site, but that no reciprocal effect exists. When the two tentoxin-binding sites are filled in reactivated F_1-ATPase, they do not exchange their role during catalytic turnover, indicating an impairment between nucleotide occupancy and the shape of tentoxin-binding pocket. This analysis provides a mechanical interpretation of the inhibition of F_1-ATPase by tentoxin and a clue for understanding the reactivation process.

F_0F_1 ATP synthases[1] are membrane-bound enzymatic complexes that couple the synthesis of ATP to the dissipation of a protonmotive force in chloroplasts, mitochondria, and bacteria (*1*). The ATP synthase can be biochemically fragmented into two different subcomplexes called F_1 and F_0. The catalytic sector F_1, with subunits α, *β*, *γ*, *δ*, and ϵ (stoichiometry $\alpha_3\beta_3\gamma_1\delta_1\epsilon_1$), is a water-soluble entity bearing catalytic and noncatalytic nucleotide binding sites, which generally retains the ability to hydrolyze ATP after isolation. The major part of X-ray structure of F_1 from mammalian mitochondria has been determined with different nucleotide occupancies (*2*−*4*). The X-ray structure of the $\alpha_3\beta_3$ nucleotide-free subcomplex from the thermophilic bacterium *Bacillus* PS3 is also known (*5*). More recently, the X-ray structure of the spinach chloroplast F_1 was partially resolved (*6*). The F_0 sector is membranous and forms a proton-channeling device converting protonmotive force into mechanical energy. Depending on species, three or more different subunits compose the F_0 moiety: $a_1b_1c_n$ in mitochondria, $a_1b_2c_n$ in bacteria, $a_1b_1b'_1c_n$ in chloroplasts, with $n = 10$ for yeast mitochondria according to X-ray crystallographic study of F_0F_1 (*7*), and $n = 14$ for spinach chloroplasts according to atomic force microscopic studies of subunit c oligomers (*8*). Mitochondrial F_0 contains additional subunits. The F_0F_1 complex is thought to act as a rotatory proton-driven motor (*9*). In the case of chloroplasts and bacteria, the stator contains subunits a, b, *δ*, α, and *β*, and the rotor contains subunits c (arranged in a crown-like structure), *γ*, and ϵ. The protonmotive force would drive the rotor in the clockwise direction when seen from the membrane, the *γ* subunit forcing the three catalytic sites to sequentially adopt the closed and open configurations

† This work was supported by the Ministère de l'Enseignement et de la Recherche (ACC-SV5 9505221, F. André) and by CNRS (Physique-Chimie du Vivant PCV97-185, F. André).

* To whom correspondence should be addressed: Service de Bioénergétique, CNRS URA 2096, CEA-Saclay, F-91191 Gif-sur-Yvette cedex, France. Tel: 33-1-69089891; fax: 33-1-69083824; e-mail: haraux@dsvidf.cea.fr.

‡ Service de Bioénergétique, DBJC.

Protéines Membranaires Transductrices d'Énergie, CNRS URA.

$ Service des Molécules Marquées, DBJC.

§ Present address: Department of Immunology, Lerner Research Institute, Cleveland, Ohio 44195, USA

¶ Present address: Molecular Modeling Group, Aventis, 102, route de Noisy, 93230 Romainville, France.

[1] Abbreviations: F_0F_1, H^+-ATP synthase complex; F_0, F_1, membranous and extrinsic subcomplexes of the H^+-ATP synthase; CF_0CF_1, chloroplast H^+-ATP synthase complex; CF_1, MF_1, TF_1, EF_1, extrinsic part of the H^+-ATP synthase complex of chloroplasts, mitochondria, *Bacillus* PS3 thermophilic bacterium and *E. coli*, respectively; CF_1-ϵ, extrinsic part of the H^+-ATP synthase complex of chloroplasts devoid of its ϵ subunit; DTT, dithiothreitol; TTX, tentoxin (*cyclo*-(L-MeAla^1-L-Leu^2-MeΔ^{Z}Phe^3-Gly^4)); ^{14}C-SBe^1-TTX, (^{14}C-benzoyl-4-benzoyl)-MeSer^1-TTX; CSB, common structural blocks; PDB, Protein Data Bank (Research Collaboratory for Structural Bioinformatics).

10.1021/bi015938z CCC: $22.00
Published on Web 04/17/2002

required by the Boyer's binding change mechanism (*1*). ATP hydrolysis is likely to result in the rotation, in the opposite direction, of the γ subunit (*10*), the ϵ subunit (*10*), and the c subunits-crown (*11*).

Tentoxin (TTX) is a natural cyclic tetrapeptide (*cyclo*-(L-MeAla[1]-L-Leu[2]-MeΔ^ZPhe[3]-Gly[4])) produced by several phytopathogenic fungi of the *Alternaria* genus (*12*, *13*), which induces chlorosis of many sensitive higher plants (*14*). TTX specifically inhibits ATP synthesis in chloroplasts of sensitive-species (*15*) as well as ATP hydrolysis in isolated CF_1 (*16*). At low concentrations ($10^{-8}-10^{-7}$ M), TTX inhibits multisite ATPase activity of isolated CF_1 (*17*), but does not affect unisite ATP hydrolysis (*18*), while at high concentrations ($10^{-5}-10^{-4}$ M) it strongly stimulates ATPase activity (*17*). A partial reactivation of the proton-transport-coupled activity of the membrane-bound CF_0CF_1 complex by high TTX concentrations was also observed (*19*). It has been reported that CF_1 binds two molecules of TTX on distinct sites (*20*, *21*) respectively related to the inhibitory and stimulatory activities of TTX, or, alternatively, that full overactivation requires binding of a third TTX molecule with a very low affinity (*22*). We have recently shown that contrary to the inhibition, the reactivation critically depends on the functional state of CF_1 and involves several forms of the enzyme, including an overactivated state and a dead-end complex unable to bind a second TTX molecule (*21*). Until now, CF_1 from sensitive species were considered as the only F_1-ATPases to be affected by TTX; this sensitivity seemed to be dependent on the Asp83 residue of the β subunit, conferring to the β subunit a decisive role in TTX binding (*23*, *24*). However, later experiments with hybrid F_0F_1 complexes assembled from TTX-resistant and TTX-sensitive species have shown that at least one copy of the α subunit from TTX-sensitive species was necessary to observe the inhibitory effect of TTX (*25*), but not its reactivatory effect (*26*). Recently, the role of the $\alpha 127-133$ segment in the TTX-inhibition was emphasized (*27*). Understanding the effects of TTX requires the localization of its binding sites, along with the determination of the tri-dimensional structure of CF_1 at high resolution. The crystal structure of $\alpha_3\beta_3$ crown from spinach chloroplast F_1-ATPase, recently published at 3.2 Å resolution (*6*), was best refined in a symmetrical conformation with all α and β subunits in a closed state, with no apparent bound adenine nucleotide and in the absence of TTX. The $\alpha\beta$ pair structure (*1fx0*) was obtained using molecular replacement based on the homologous structure of the bovine mitochondrial enzyme, and did not allow one to precisely describe the TTX-binding site (*6*).

The mechanism by which TTX inhibits and reactivates the CF_1-ATPase is therefore still unknown. The present report focuses on three aspects of this mechanism: (i) the molecular basis of the sensitivity to TTX; (ii) the process by which TTX could block the catalytic cycle, in the frame of the Boyer's sequential binding change mechanism; (iii) the interaction between the inhibitory and the reactivatory TTX binding sites. We used different biochemical approaches (binding experiments, kinetic studies, photochemical, and isotopic labeling) along with molecular modeling. The question of TTX specificity, that is closely related to the structure of the TTX-binding site, was addressed by studying the effects of TTX on non-chloroplast F_1-ATPases, knowing that mitochondrial and bacterial F_1-ATPases were considered as TTX-insensitive so far. We actually found that TF_1-ATPase from *Bacillus* PS3 was inhibited by TTX, while MF_1-ATPase from various species remained resistant to TTX. Using a photoactivatable TTX analogue, we found that TTX specifically binds the α subunit of CF_1-ϵ. We then docked TTX in its putative site located at the three possible α/β interfaces of a rebuilt 3D structure of CF_1 $\alpha_3\beta_3\gamma$ subcomplex, made asymmetrical after insertion of γ subunit (*28*). Kinetic experiments performed on CF_1-ϵ using well-characterized TTX analogues as competitors revealed how the inhibitory site influences the reactivatory site, whereas chase experiments using ^{14}C-labeled TTX showed that the reactivatory site has no influence on the binding properties of the inhibitory site. In this report, we propose the first mechanistic model of F_1-ATPase inhibition by a single TTX molecule, and we specify some key features of the mechanism of reactivation by a second TTX molecule.

EXPERIMENTAL PROCEDURES

Materials. The soluble thermophilic bacterium ATPase (TF_1) was purified from cells of PS3 *Bacillus* as described (*29*), and the soluble chloroplast ATPase devoid of ϵ subunit (CF_1-ϵ) was purified from spinach leaves as described (*30*). Protein concentration was determined by UV absorption spectroscopy (*31*, *32*).

Ser[1]-TTX, Ser(Bn)[1]-TTX, Glu(tBu)[1]-TTX, Lys[2]-TTX, Lys(Z)[2]-TTX, Tyr[3]-TTX, and Tyr(Me)[3]-TTX were synthesized by Drs. Florine Cavelier and Jean Verducci, CNRS-UMR 5810, Université Montpellier II, France, as in ref *33*. Dihydro-TTX and Iso[3]-TTX were provided by Dr Bernd Liebermann, Biologisch-Pharmazeutische Fakultät der Friedrich-Schiller-Universität Jena, Germany. Ala[1]-TTX, Sar[1]-TTX, Gly[1]-TTX, ΔPhe[3]-TTX and TTX were synthesized in the laboratory.

Binding Experiments with ^{14}C-TTX. ^{14}C-TTX was prepared with a specific activity of 52 Ci mol^{-1} (*20*). For binding experiments with TF_1, 100 μL samples of TF_1 at 2 or 6 μM, depending on TTX concentration, were incubated for 3 to 5 h with ^{14}C-TTX (from 5 to 700 μM) in 50 mM Tris-SO_4, pH 8, 60 °C. After reaching of binding equilibrium, bound and free TTX were rapidly separated on a PD10 Pharmacia column at room temperature. The ^{14}C radioactivity of every eluted fraction was counted twice for 5 min using a Beckman LS 3801 scintillation counter. It ranged between 150 ± 20 and 10^5 cpm.

For the experiments of TTX exchange, CF_1-ϵ preactivated with 3 mM DTT was incubated for 3 h at a concentration of 1 μM with 300 nM ^{14}C-TTX in 50 mM Tris-SO_4, pH 8, at 37 °C. The exchange of ^{14}C-TTX was initiated by adding 50 μM cold TTX. Aliquots were taken up at different times after cold TTX addition, and the free and bound ^{14}C-TTX were separated and counted as above.

Steady-State Measurement of ATPase Activity. CF_1-ϵ, preincubated for at least 3 h at 20 °C with 3 mM DTT plus 20 mM Tricine, pH 8, was diluted at 2−5 nM in 50 mM Tris-SO_4, 40 mM $KHCO_3$, and 0.18 mM $MgSO_4$, pH 8, 37 °C. Then TTX or analogues were added at indicated concentrations. The reaction was initiated by adding ATP after a time (5 to 120 min) depending on toxin concentration, to reach binding equilibrium conditions.

For TF_1, the temperature of the reaction medium was 60 °C. TF_1-ATPase 2 nM was incubated with TTX or analogues

Table 1: Rate Constant of Association (k_{on}), Equilibrium Constant of Dissociation (K_d), and Rate Constant of Dissociation (k_{off}) of TTX and Different Analogues on the Inhibitory Site of CF_1-ϵ[a]

name	formula	k_{on} (M^{-1} s^{-1})	K_d (M)	k_{off} (s^{-1})	% inhibit
TTX	*cyclo*-(L−*N*-methyl-Ala[1]-L-Leu[2]−*N*-methyl-Δ^ZPhe[3]-Gly[4])	4.7×10^4	8.0×10^{-9}	3.7×10^{-4}	>95
Ala[1]-TTX	*cyclo*-(**L-Ala[1]**-L-Leu[2]-*N*-methyl-Δ^ZPhe[3]-Gly[4])	1.7×10^4	3.4×10^{-8}	6.1×10^{-4}	>95
Sar[1]-TTX	*cyclo*-(**L−*N*-methyl-Gly[1]**-L-Leu[2]-*N*-methyl-Δ^ZPhe[3]-Gly[4])	4.8×10^4	4.5×10^{-8}	2.1×10^{-3}	80
Gly[1]-TTX	*cyclo*-(**L-Gly[1]**-L-Leu[2]-*N*-methyl-Δ^ZPhe[3]-Gly[4])	5.0×10^4	3.4×10^{-8}	1.7×10^{-3}	75
Ser[1]-TTX	*cyclo*-(**L−*N*-methyl-Ser[1]**-L-Leu[2]-*N*-methyl-Δ^ZPhe[3]-Gly[4])	3.7×10^4	1.5×10^{-8}	5.5×10^{-4}	>95
Ser(Bn)[1]-TTX	*cyclo*-(**L−*N*-methyl-Ser(Bn)[1]**-L-Leu[2]-*N*-methyl-Δ^ZPhe[3]-Gly[4])	2.2×10^4	5.0×10^{-7}	1.1×10^{-2}	>95
Glu(tBu)[1]-TTX	*cyclo*-(**L−*N*-methyl-Glu(tBu)[1]**-L-Leu[2]-*N*-methyl-Δ^ZPhe[3]-Gly[4])	3.3×10^3	1.5×10^{-6}	5.0×10^{-3}	>95
Lys[2]-TTX	*cyclo*-(L−*N*-methyl-Ala[1]-**L-Lys[2]**−*N*-methyl-Δ^ZPhe[3]-Gly[4])	4.2×10^2	2.0×10^{-6}	8.4×10^{-4}	>95
Lys(Z)[2]-TTX	*cyclo*-(L−*N*-methyl-Ala[1]-**L-Lys(Z)[2]**−*N*-methyl-Δ^ZPhe[3]-Gly[4])	5.0×10^3	7.5×10^{-7}	3.5×10^{-3}	>95
Tyr[3]-TTX	*Cyclo*-(L−*N*-methyl-Ala[1]-L-Leu[2]-***N*-methyl-Δ^ZTyr[3]**-Gly[4])	1.5×10^4	1.2×10^{-8}	1.8×10^{-4}	>95
Tyr(Me)[3]-TTX	*cyclo*-(L−*N*-methyl-Ala[1]-L-Leu[2]-***N*-methyl-Δ^ZTyr(Me)[3]**-Gly[4])	1.3×10^4	1.0×10^{-8}	1.3×10^{-4}	>95
ΔPhe[3]-TTX	*cyclo*-(L−*N*-methyl-Ala[1]-L-Leu[2]-**Δ^ZPhe[3]**-Gly[4])	7.0×10^2	8.0×10^{-7}	5.6×10^{-4}	>95
dihydro-TTX	*cyclo*-(L−*N*-methyl-Ala[1]-L-Leu[2]-***N*-methyl-Phe[3]**-Gly[4])	1.5×10^4	5.0×10^{-7}	7.5×10^{-3}	90
Iso[3]-TTX	*cyclo*-(L−*N*-methyl-Ala[1]-L-Leu[2]-***N*-methyl-Δ^EPhe[3]**-Gly[4])	1.7×10^3	8.7×10^{-6}	5.1×10^{-3}	90

[a] All constants were determined from activity measurements, as described under Experimental Procedures (see also ref *21*). The last column indicates the maximal extent of inhibition. k_{on} was deduced from time-resolved experiments, K_d was from steady-state experiments, and k_{off} was indirectly estimated as the K_d k_{on} product.

in the reaction medium for 1−8 h, depending on toxin concentration, to reach binding equilibrium. 40 mM $KHCO_3$ and 0.18 mM $MgSO_4$ were added 5 min before initiating ATP hydrolysis by 1 mM ATP addition.

ATPase activity was measured using HPLC technique as described (*34*). Control activities were 10 to 15 μmol of ATP min^{-1}/mg of protein for TF_1 (60 °C) and 4 to 6 μmol of ATP min^{-1}/mg of protein for CF_1-ϵ (37 °C).

Time-Resolved Assays of ATPase Activity. For kinetic study of inhibition of TF_1, the enzyme (1 nM) was incubated for 10 min in a spectrophotometric cuvette, stirred, and thermostated at 50 °C, containing 50 mM Tris-SO_4, pH 8, 40 mM $KHCO_3$, 0.2 mM $MgSO_4$, and enzymatic system coupling ATP hydrolysis to NADH oxidation, monitored at 340 nm (*21*). ATP hydrolysis was started by adding 2 mM MgATP to the reaction medium. TTX was either added 5 min later, or incubated with TF_1 at different times before MgATP addition.

Kinetic study of inhibition of CF_1-ϵ (Table 1) was carried out as in ref *21*. For kinetic study of reactivation of CF_1-ϵ (Figures 5−6), 10 nM of DTT-treated CF_1-ϵ was incubated for 10 min with the first toxin at the indicated inhibitory concentration in the reaction medium. ATP hydrolysis was started by adding 2 mM MgATP. After 3 min, TTX was added at high concentrations, and the reactivation could be observed.

Photolabeling Experiments. (^{14}C-benzoyl-4-benzoyl)-MeSer[1]-TTX was synthesized as reported (*35*). CF_1 and (^{14}C-benzoyl-4-benzoyl)-MeSer[1]-TTX were mixed at the indicated concentrations in 50 mM Tris-SO_4, pH 8.0, under argon. The sealed sample was incubated in darkness for 3 h at 15 °C, and then irradiated at 364 nm at the indicated intensity and for the indicated time. After the irradiation, the sample (0.5 to 2 mL) was dialyzed (membrane cutoff = 12 kDa) 2 times for 12 h against 2 L of 50 mM Tris-SO_4, pH 8.0, at 5 °C and in darkness, then dialyzed 2 times for 12 h at room temperature against 50 mM ammonium bicarbonate, pH 7.75, 0.2% SDS. The sample was then electrophoretically analyzed and revealed by Coomassie blue and ^{14}C radioactivity. Densitometric analysis of gels and autoradiograms was made using a Gel Doc 1000 system (Biorad).

Molecular Modeling. A 3D model of spinach $\alpha_3\beta_3\gamma$ interacting with TTX has been built using an original homology modeling technique (*28*). Common structural blocks (CSB) of the X-ray structures of TF_1, bovine MF_1 and rat MF_1 (PDB files 1sky, 1bmf, and 1mab, respectively) were deduced from similar (ϕ, ψ) trajectories of the homologous polypeptide chains of these three structures in internal coordinates space. This was achieved using a local structural alignment search tool (GOK software, ABI, Université Paris VI). Structure calculation was performed using DYANA software, and further optimization (as defined by PROCHECK analysis) made by XPLOR software, with the topology and parameter files of CHARM22 force field. α and β chains were rebuilt separately, and then assembled under XPLOR-CHARM22 optimization. The asymmetry of $\alpha\beta$ pairs, relative to their nucleotide occupancy (ATP, ADP, empty), was introduced at this step, using constraints derived from internal CSB analysis of *1bmf*. The fragments of γ subunit found in *1bmf* were rebuilt by sequence homology and introduced into the structure. After final assembly, an asymmetrical model of chloroplast $\alpha_3\beta_3\gamma$ was obtained (*28*). TTX docking was initiated by placing TTX into the presumed binding site, in the vicinity of βAsp83 and at the α/β interface of each $\alpha\beta$ pair. Sixty random shifts were applied to the TTX molecule, which decomposed into three random rotations and one random translation lower than 15 Å. CF_1/TTX complex was then optimized under XPLOR-CHARM22 energy minimization restricted to a 17-Å radius sphere centered on TTX.

RESULTS

Photolabeling of the TTX-Binding Site. We have synthesized the photoactivatable TTX derivative (^{14}C-benzoyl-4-benzoyl)-MeSer[1]-TTX (Scheme 1), which has been characterized for its photoactivatable properties (*35*). It inhibited CF_1-ϵ with a K_d of 5 μM (data not shown). Irradiation experiments of CF_1 in the presence of (^{14}C-benzoyl-4-benzoyl)-MeSer[1]-TTX were carried out and resulted in irreversible incorporation of ^{14}C into the protein. Figure 1 shows the radioactivity profiles of SDS−PAGE gels obtained for different times of irradiation. The radioactivity is mainly located on the α subunit, with minor labeling of β, γ, δ,

Scheme 1: Structure of ^{14}C-tentoxin and (^{14}C-benzoyl-4-benzoyl)-MeSer^1-TTX[a]

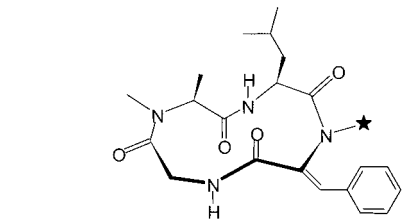

^{14}C-TTX

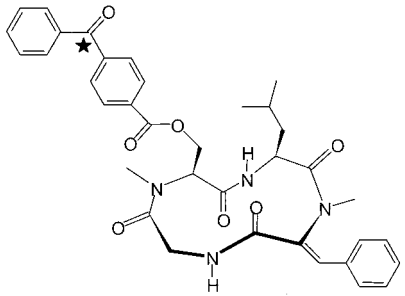

(^{14}C-benzoyl-4-benzoyl)-MeSer^1-TTX

[a] The position of the radioactive carbon is indicated by a star.

and ϵ, as can be deduced from the densitograms of Coomassie blue and radioactivity. Figure 2 shows radioactivity profiles drawn from autoradiograms obtained at low intensity and short times of irradiation, in the absence and in the presence of cold TTX at high concentration. These radioactive profiles, focused on the α and β subunits, show that the incorporation of ^{14}C was lower than in Figure 1, as expected. It can be seen that, in the presence of a high concentration of cold TTX, the incorporation of ^{14}C is preserved on the β subunit, but not on the α subunit. We conclude that the labeling of β is essentially nonspecific, and that TTX and its photoactivatable analogue specifically bind on a site that is located on the α subunit. This result puts into question the early view attributing to β subunit the major role in the TTX-sensitivity of the chloroplast ATPase (*23*, *24*) but is in accordance with more recent results reevaluating the importance of the α subunit for the inhibition of CF_1 by TTX (*25*−*27*).

Modeling the TTX-Binding Inhibitory Site. Photolabeling experiments clearly demonstrate that TTX binds to the α subunit of CF_1, but at the same time it makes no doubt that some residues of the β subunits, and more especially βAsp83, are involved in sensitivity to TTX (*23*−*25*). This strongly supports the location of the inhibitory TTX-binding site at an interface between α and β, not far from βAsp83 (*6*, *25*−*27*). Besides, the presence of γ subunit is required for TTX binding at a high affinity site (*36*), suggesting that this subunit induces a conformation suitable for heterogeneous binding of TTX to αβ interface. To produce a reliable model of the inhibitory TTX-binding site, we thus built an asymmetrical structure of the $\alpha_3\beta_3\gamma$ CF_1 subcomplex. Since the PDB file (*1fx0*) corresponding to the published αβ CF_1 crystal structure was still on hold during the modeling work, we used the tridimensional structures of mammalian MF_1 (*2*, *3*), EF_1 (*37*) and PS3 αβ pairs (*5*) to build our model (*28*). It was possible to dock TTX under the various conformations

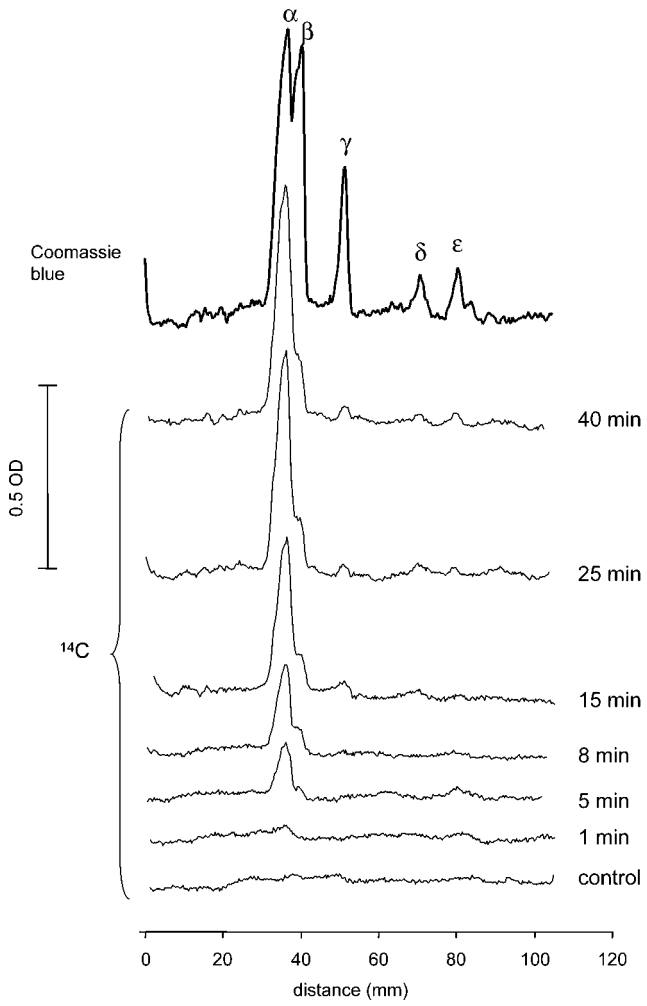

FIGURE 1: Autoradiogram profiles of SDS−PAGE of CF_1 photolabeled with (^{14}C-benzoyl-4-benzoyl)-MeSer^1-TTX. Conditions as described under Experimental Procedures. Concentrations during irradiation: CF_1, 8 μM; ^{14}C-SBe^1-TTX, 4 μM. Intensity of irradiation, 2 mW cm^{-2}. Times of irradiation are indicated. Top part of the figure, corresponding protein density profile with Coomassie blue dyeing showing the five subunits.

previously determined by NMR (*38*) into the putative inhibitory binding site. The starting positions of TTX in docking calculations were chosen in accordance with specific photolabeling of the α subunit and with the early recognized importance of βAsp83 in TTX sensitivity (*23*−*24*). The docking runs revealed that the inhibitory site is essentially formed by a hydrophobic pocket of conserved aromatic residues of the α subunit (αTyr237, αTyr241, αTyr271, and αTyr293) surrounded by several charged residues (αGlu131, αArg297, αArg301). The pocket opens onto the β subunit at the level of βAsp83. Several slightly different positions of TTX within this cavity were found on the basis of energetic calculations, due to the presence of multiple hydrogen donors and acceptors on both the TTX backbone and the side chains of the α subunit. Figure 3 shows the prevalent position found for the conformer A of TTX (*38*) in the nucleotide-free reconstructed α/β interface. The TTX molecule can establish the following interactions: NH group of TTXLeu2 with αGlu131 and αTyr241 (through hydrogenbonding), C═O group of TTXLeu2 with αTyr293 (hydrogen bond), C═O group of TTXMeAla1 with αArg297 (hydrogen bond); the aromatic ring of TTXΔPhe3 is likely

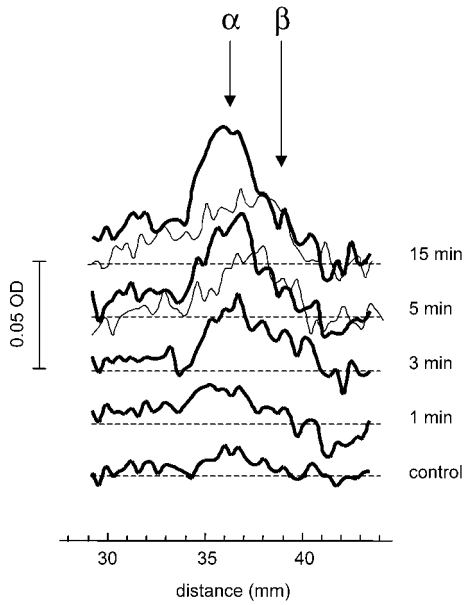

FIGURE 2: Autoradiogram profiles of CF_1 photolabeled with (^{14}C-benzoyl-4-benzoyl)-MeSer^1-TTX in the absence and presence of cold TTX. Conditions as described under Experimental Procedures (see also Figure 1). 2 μM CF_1, 8 μM ^{14}C−SBe^1-TTX. Thick lines, no cold TTX. Thin lines, 800 μM cold TTX. Intensity of irradiation, 50 μW cm^{-2}. Times of irradiation are indicated.

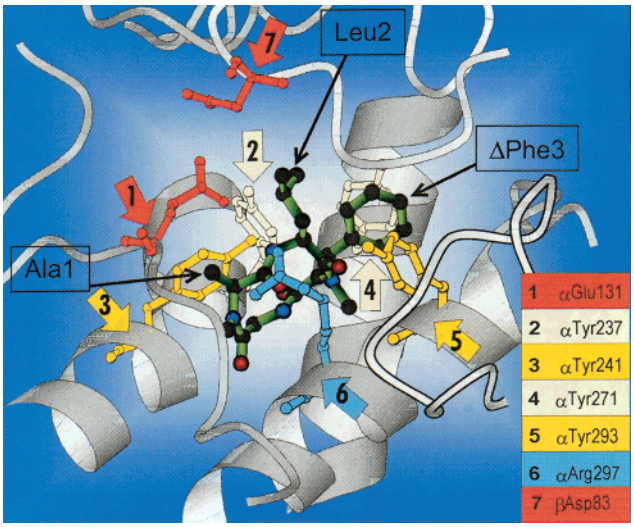

FIGURE 3: Position of tentoxin in the binding site of nucleotide-free $\alpha\beta$ pair of CF_1. The inhibitory binding site of TTX at the α/β interface associated to the nucleotide-free catalytic site, as derived from docking calculations in the reconstructed 3D asymmetric structure of spinach $\alpha_3\beta_3\gamma$ ATPase subcomplex. The positioning of the molecule corresponds to the lowest free energy of interaction. Bottom of the figure corresponds to the direction toward the membrane. The skeleton of CF_1 is in gray, and the backbone of TTX is in green, with heteroatoms represented with their standard color codes. Hydrogen atoms are not represented. Six CF_1 amino acids, expected to interact with TTX, are represented. They all belong to the α subunit. The βD83 residue, thought to confer the TTX sensitivity, is also represented (Adapted from MOLSCRIPT).

to stack with the ring of αTyr271. Conversely, the conformer B of TTX in which the MeAla−Leu peptide bond is inverted (*38*) can establish the following H bonds: NH group of TTXLeu2 with αArg297, C═O group of TTXLeu2 with αTyr293, and C═O group of TTXMeAla1 with αTyr241.

Docking runs of the TTX molecule on the three different α/β interfaces of the asymmetrical model of CF_1 were performed. It was found that the TTX molecule could be positioned with similar increases of global energy in the potential binding sites of nucleotide-free and ADP-loaded $\alpha\beta$ pairs, and disfavored in the homologous site of the ATP-loaded $\alpha\beta$ pair. Energy calculations[2] of the protein−ligand complexes (*28*) indeed revealed that in the case of nucleotide-free and ADP-loaded $\alpha\beta$ pairs, binding of TTX resulted in energy increase of 75 ± 20 kcal/mol (averaged on 20 complexes of lowest energy among 60 docking cycles) for the nucleotide-free $\alpha\beta$ pair, and 65 ± 20 kcal/mol (averaged on 20 complexes of lowest energy among 60 docking cycles) for the ADP-loaded $\alpha\beta$ pair. But for the ATP-loaded $\alpha\beta$ pair, no satisfactory docking was found in 60 cycles (the energy increase found was at least 1000 kcal/mol). This indicates that binding TTX on the ATP-loaded $\alpha\beta$ pair in the same cavity as in the ADP-loaded and nucleotide-free pairs is too energetically costly to be favored. We think that this feature has implications for the mechanism of TTX inhibition, as it will be explained below.

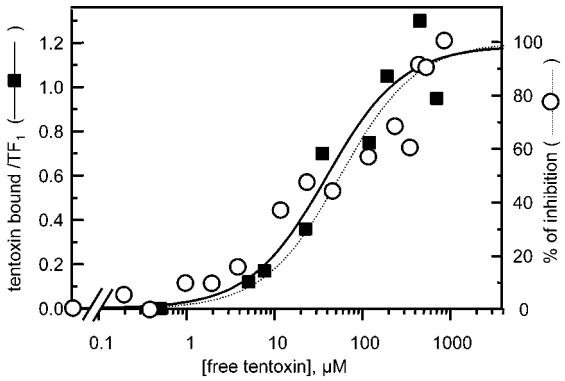

FIGURE 4: Binding of TTX to TF_1 and inhibitory effect. Conditions as described under Experimental Procedures. Closed squares, TTX bound per TF_1 as a function of free TTX concentration; open circles, inhibition of ATPase activity as a function of free TTX concentration. See text for details.

Inhibition of TF_1-ATPase by Tentoxin and Effect of ATP on the Tentoxin Binding Rate. Until now, it was considered that nonphotosynthetic F_1-ATPases were TTX insensitive. This was proved in the case of *Escherichia coli* ATPase (*39*), but only poorly documented in the case of MF_1 (*40*). We have verified that TTX at concentrations ranging from 10^{-8} to 10^{-4} M had no effect on MF_1 from three different sources (rat liver, beef heart, and yeast; data not shown). We have also investigated the effect of TTX on the bacterial TF_1-ATPase. At 60 °C, TF_1-ATPase proved to be inhibited by TTX with a calculated K_I comprised between 30 and 60 μM (Figure 4). Experiments using ^{14}C-labeled TTX under similar conditions confirmed that TTX binds to TF_1-ATPase. The data supported a simple binding model with a unique class of sites, with $K_d = 39 \pm 14$ μM and $n = 1.2 \pm 0.1$ binding site per TF_1 molecule (Figure 4). Therefore TF_1, as CF_1, is inhibited by the binding of a single TTX molecule, but the affinity constant of TTX for the inhibitory site is about 5000 times lower than in the case of CF_1 (K_I is about 10 nM for CF_1, devoid or not of the ϵ subunit (*21*)). Inhibition of TF_1 by TTX was observed only at a high temperature: at 37 °C,

[2] As all the energies derived from force-field calculations, these energy values cannot be considered as absolute and cannot be used to calculate dissociation constants. Only their comparison is relevant.

practically no inhibitory effect was observed up to 1 mM TTX (data not shown).

Since ^{14}C-binding experiments were carried out in the absence of ATP, the presence of added nucleotides is not a prerequisite for TTX binding to TF_1, as previously observed for CF_1 (*21*). In that early work, it was also shown, by kinetic experiments using coupled assay (NADH oxidation), that even the rate of binding of TTX to the inhibitory site of CF_1-ϵ did not depend on the presence of ATP. We have repeated with TF_1 these time-resolved experiments, at 50 °C and with 20 μM TTX. When ATP was present before TTX, the rate of ATP hydrolysis rapidly decayed upon TTX addition, 50% of the inhibition process being achieved within 40 s. When ATP was added only at different times after TTX to reveal the remaining ATPase activity, the rate of inhibition by TTX was dramatically decreased, at least 6−7-fold (data not shown). This result is quite different from that previously obtained with CF_1-ϵ, where the rate of inhibition did not depend on the presence of ATP (*21*). As it will be discussed below, these different patterns could be ascribed to the different nucleotide contents of isolated TF_1 and CF_1-ϵ. Using our standard procedures of isolation, these contents are 0.75 ± 0.25 ADP molecule per CF_1 molecule and 0.08 ± 0.01 ADP molecule per TF_1 molecule (*41*).

Steady-State Reactivation of CF_1-ϵ Depending on the Toxin Bound on the Inhibitory Site. The second key property of TTX is its ability to reactivate CF_1-ATPase at high concentration. In a previous study, we had shown that some TTX analogues were able to bind the reactivatory site of CF_1-ϵ without restoring any ATPase activity (*42*). Other analogues, once bound to the two sites, gave ATPase complexes reactivated to different levels (*42*, *34*). Competition experiments on the low affinity site also indicated that the activity of the ATPase complex bearing two toxin molecules depended not only on the nature of the toxin bound to the reactivatory site, but also on the nature of the toxin bound to the inhibitory site (*34*). This proved that an interaction exists between the two TTX binding sites, but it could not be determined whether the binding of the first toxin molecule was also able to modulate the affinity of the reactivatory site for a second molecule. This can be achieved by using an appropriate combination of toxins, and to reach this goal, we have synthesized a number of TTX analogues and checked them for their binding parameters k_{on}, K_d, and k_{off} to the inhibitory site, using the method developed in ref *21* for natural TTX. The results are displayed in Table 1. Three TTX analogues were then selected for studies on reactivation: Lys(Z)^2-TTX, Sar^1-TTX, and Ser^1-TTX.

In Figure 5a, the normalized rate of ATP hydrolysis catalyzed by CF_1-ϵ was plotted as a function of the concentration of Lys(Z)^2-TTX. The data could be fitted using the previously developed two-sites model (*34*), which allowed us to determine three parameters: the dissociation constant of Lys(Z)^2-TTX from the inhibitory site (K_{d1}), its dissociation constant from the activatory site (K_{d2}), and the activity of the ATPase complex bearing two Lys(Z)^2-TTX molecules (V_A). The fit gave $K_{d1} = 0.7$ μM, $K_{d2} = 15$ μM, and $V_A = 30\%$ of the activity of the toxin-free ATPase complex. With the natural toxin TTX, $K_{d1} = 0.008$ μM, $K_{d2} = 38$ μM, and $V_A = 240\%$ of the control (*21*, *34*).

Figure 5b shows the normalized rate of ATP hydrolysis as a function of the concentration of Lys(Z)^2-TTX, now in the presence of 20 μM of the natural toxin TTX. In this condition, about 30% of the ATPases initially bear two TTX molecules and are highly active. The activity decreases when the concentration of Lys(Z)^2-TTX increases, mainly because TTX is progressively replaced by Lys(Z)^2-TTX on the reactivatory site. The data of Figure 5b could be fitted using a competitive model (Figure 5c). The different possible catalytic states of ATPase are actually the following: E, the

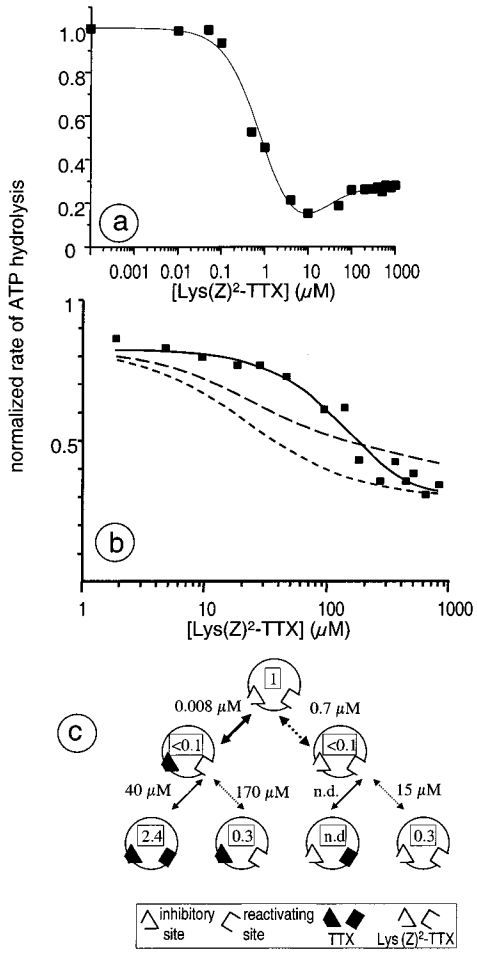

FIGURE 5: Effect of Lys(Z)^2-TTX on the ATPase activity of CF_1-ϵ in the absence and in the presence of tentoxin at reactivatory concentration. Conditions as described under Experimental Procedures. (a) No TTX; the curve was drawn from the fit obtained with the theoretical two-sites model (*21*, *33*), with $K_L = 0.7$ μM, $K_{LL} = 15$ μM, and $V_{LL} = 0.3$ (see text for details). (b) 20 μM TTX present; the dotted curve was drawn using the two-sites model, and by assuming that the nature of the toxin bound on the tight site influences neither the dissociation constant of the loose site for another toxin, nor the activity of the ternary complex bearing two toxin molecules; the dashed curve was obtained by assuming that the nature of the toxin bound on the tight site influences the activity of the ternary complex, but not the dissociation constant of the loose site; the solid curve was obtained by assuming that the nature of the toxin bound on the tight site influences both the activity of the ternary complex and the dissociation constant of the loose site. (c) Interpretation of the data in terms of affinity of the inhibitory and reactivating sites for the two different toxins; top, no toxin bound; middle, one toxin molecule bound; bottom, two toxin molecules bound; the normalized activities of the different complexes are indicated within the circles; these activities as well as the K_d's of the different equilibria are drawn from the data displayed in panels a and b. Note that the K_d of Lys(Z)^2-TTX at the reactivating site is 170 μM when the inhibitory site is occupied by TTX, and 15 μM when the inhibitory site is occupied by Lys(Z)^2-TTX.

toxin-free enzyme; ET, the enzyme inhibited by one TTX molecule; ETT, the enzyme bearing two TTX molecules; EL, the enzyme inhibited by one Lys(Z)^2-TTX molecule; and ELL, the enzyme bearing two Lys(Z)^2-TTX molecules. In addition, two other states must be considered: ETL, which bears one TTX molecule on the inhibitory site and one Lys(Z)^2-TTX molecule on the reactivatory site; and ELT, which bears one Lys(Z)^2-TTX molecule on the inhibitory site and one TTX molecule on the reactivatory site. The catalytic activities of the different states are the following: 1 for the E state, 0 for the EL and the ET state, V_{TT} for the ETT state, V_{TL} for ETL, etc. In this case, the normalized rate of ATP hydrolysis can be expressed by the following equation:

$$V = [E] + V_{TT}[ETT] + V_{TL}[ETL] + V_{LT}[ELT] + V_{LL}[ELL] \quad (1)$$

where [E], [ETT], [ETL], [ELT], and [ELL] represent the proportions of the corresponding states. These proportions depend on TTX concentration, Lys(Z)^2-TTX concentration, and six dissociation constants: K_T and K_L, the dissociation constants of TTX and Lys(Z)^2-TTX from the inhibitory site, previously determined; K_{TT} and K_{LL}, the dissociation constants of TTX and Lys(Z)^2-TTX from the reactivatory site when the inhibitory site is occupied by the same toxin (these constants are also known); and K_{LT} and K_{TL}, the dissociation constants of TTX and Lys(Z)^2-TTX from the reactivatory site, respectively, when the inhibitory site is occupied by the other toxin. These dissociation constants of heterologous complexes were not a priori known and could be determined by fitting the data of Figure 5b using the equations developed in ref *34*. The dotted theoretical curve is that obtained by assuming that the binding constant of each toxin on the loose site and the resulting level of reactivation do not depend on the nature of the toxin bound on the tight site ($K_{LT} = K_{TT}$, $K_{TL} = K_{LL}$, $V_{LT} = V_{TT}$ and $V_{TL} = V_{LL}$). It clearly does not match the data, which confirms that some information is transmitted from the tight site to the loose site. The dashed theoretical curve shows what happens if one keeps the binding constants K_{LT} and K_{TL} unchanged (that is $K_{LT} = K_{TT}$ and $K_{TL} = K_{LL}$) but allows the activities of the heterologous ELT and ETL complexes to be independently determined. Obviously, the model does not yet match the data. Finally, the continuous curve was obtained by allowing the heterologous binding constants and activities to vary. The data were correctly fitted and gave $K_{TL} = 170$ μM and $V_{TL} =$ 28%. Not surprisingly, the result of the fit is practically insensitive to the values of K_{LT} and V_{LT}, because the contribution of the ELT state, bearing one Lys(Z)^2-TTX molecule on the inhibitory site and one TTX molecule on the reactivatory site, is negligible. Consequently, the parameters K_{LT} and V_{LT} could not be determined.

The main result deduced from these competition experiments is the following: the K_d of Lys(Z)^2-TTX for the reactivatory site is 15 μM when the inhibitory site is occupied by Lys(Z)^2-TTX, and 170 μM when the inhibitory site is occupied by TTX. The scheme of Figure 5c summarizes the parameters derived from the different fits.

Rate of CF$_1$-ϵ Reactivation by Tentoxin Depends on the Toxin Bound on the Inhibitory Site. Since all the TTX derivatives analyzed show a lower affinity than TTX for the inhibitory site of CF$_1$-ϵ, it is practically impossible, in steady state experiments, to bind a molecule of TTX analogue on the inhibitory site and a molecule of natural TTX on the reactivatory site. This can be achieved only in kinetic experiments, by preincubating the enzyme with a TTX analogue at inhibitory concentrations, and then adding TTX at high concentration. Depending on the k_{off} of the toxin bound at the inhibitory site, which is generally low, it is then possible to observe during a significant period the TTX-induced reactivation of enzymes bearing another toxin on the inhibitory site. Figure 6 shows such kinetics of reactivation obtained by adding TTX at different concentrations to CF$_1$-ϵ previously inhibited by Lys(Z)^2-TTX (6a), Sar^1-TTX (6b), and Ser^1-TTX (6c). It can be seen that the kinetic profiles depend on the toxin bound on the first site, but the differences become more evident on the secondary plots drawn from data of Figure 6 and displayed in Figure 7. Plots 7a, 7b, and 7c show, for different times after TTX addition (15, 45, and 90 s, respectively), the ATPase activity as a function of the TTX concentration. During this time interval the exchange of toxin at the level of the inhibitory site is negligible. At any time, the activity not only depends on

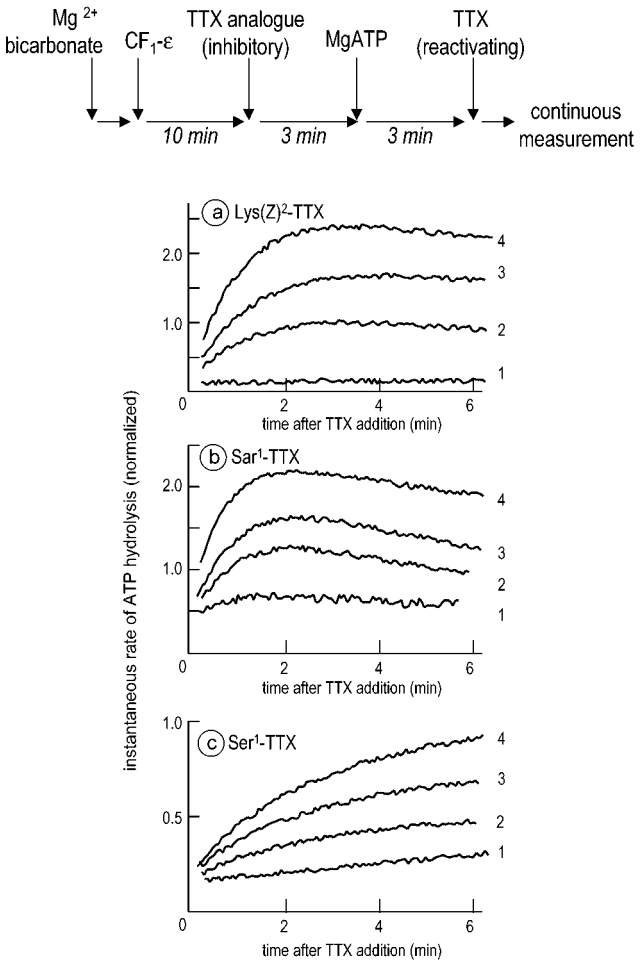

FIGURE 6: Kinetics of CF$_1$-ϵ ATPase reactivation by tentoxin with different analogues bound on the inhibitory site. Conditions as described under Experimental Procedures (see also the top of the figure). The traces represent instantaneous rates of ATP hydrolysis as a function of the time, directly drawn from the first derivative of spectrophotometric recording. (a) Lys(Z)^2-TTX 10 μM; traces 1 to 4, TTX 5 μM, 50 μM, 100 μM, 200 μM. (b) Sar^1-TTX 0.5 μM; traces 1 to 4, TTX 5 μM, 25 μM, 50 μM, 150 μM. (c) Ser^1-TTX 0.5 μM; traces 1 to 4, TTX 30 μM, 75 μM, 100 μM, 150 μM.

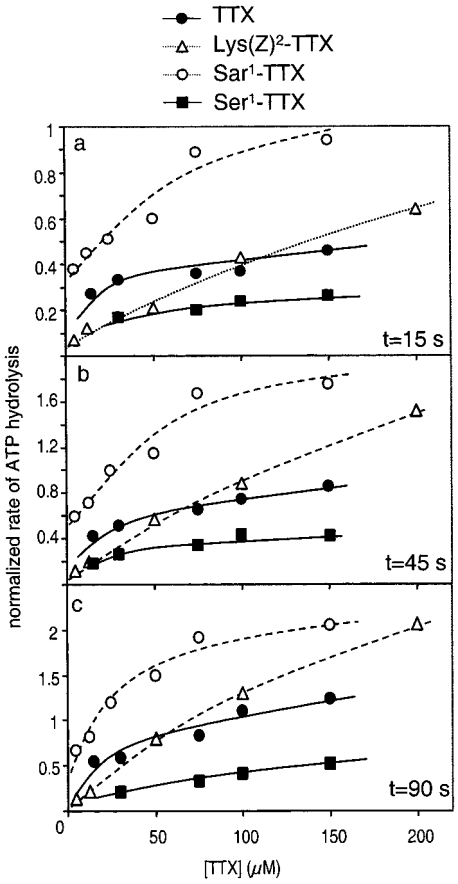

FIGURE 7: Rates of ATP hydrolysis by CF_1-ϵ inhibited with different tentoxin analogues and reactivated by tentoxin. Secondary plots drawn from the data of Figure 6. (a) Rates of ATP hydrolysis as a function of the TTX concentration, 15 s after TTX addition. (b) Rates of ATP hydrolysis as a function of the TTX concentration, 45 s after TTX addition. (c) Rates of ATP hydrolysis as a function of the TTX concentration, 90 s after TTX addition. Toxin on the inhibitory site are TTX (●) (data from ref *21*), Lys(Z)²-TTX (△), Sar¹-TTX (○), and Ser¹-TTX (■).

TTX concentration, but more critically depends on the nature of the toxin present on the inhibitory site. This result completes the observations made in steady-state experiments with the natural toxin bound at the tight site. It confirms that the inhibitory TTX-binding site exerts an influence on the reactivatory site, by modulating its affinity for natural TTX or TTX derivatives.

Filling the Reactivatory Loose Site Does Not Change the Binding Properties of the Inhibitory Tight Site. Since filling the tight site modulates the affinity of the loose site, the question arises to know whether this interaction is reciprocal and whether TTX binding on the reactivatory site may influence the TTX affinity of the inhibitory site. We have therefore investigated the effect of TTX binding on the loose site on the rate of TTX exchange on the inhibitory site. First, the kinetics of release of TTX from the first site was analyzed by triggering and measuring the rate of ATP hydrolysis by TTX-inhibited CF_1-ϵ at different times after dilution in a medium devoid of TTX and ATP (data not shown). Under these conditions, the k_{off} could be estimated as $3 \pm 1\ 10^{-4}$ s^{-1}, almost the same value as that deduced from the values of K_d and k_{on} determined in the presence of ATP ($3.7\ 10^{-4}$ s^{-1}; ref *21*; see also Table 1). To follow the rate of TTX exchange on the tight site in the presence of high TTX

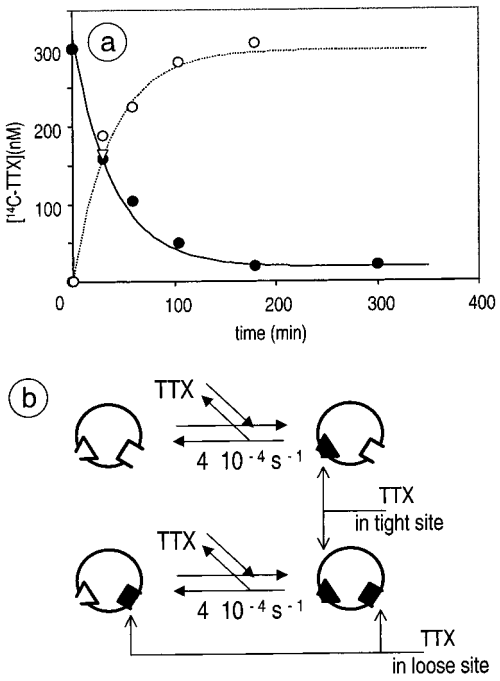

FIGURE 8: Rate of exchange of TTX on the inhibitory site after filling of the reactivating site. (a) Concentration of bound and free ^{14}C-TTX at different times after addition of cold TTX to ^{14}C-loaded CF_1-ϵ. Conditions as described under Experimental Procedures. Concentration of cold TTX: 50 μM. (●) Bound ^{14}C-TTX in the absence of MgATP; (○) Free ^{14}C-TTX in the absence of MgATP; (▽) free ^{14}C-TTX in the presence of MgATP 5 mM. (b) Interpretation; occupied TTX-binding sites are in black, the rate constant of dissociation of TTX from the inhibitory site is indicated.

concentration, we partially filled this site using a substoichiometric concentration of ^{14}C-TTX. Then, the exchange was initiated by addition of cold TTX at reactivating concentration (50 μM), and followed by separating free ^{14}C-TTX from bound ^{14}C-TTX at different times after cold TTX-addition. Figure 8a shows the amounts of free and bound ^{14}C-TTX as a function of time. The two kinetics were fitted by a monoexponential function with a unique time constant, representing the dissociation rate constant of TTX from the tight site. It was found to be $4.0 \pm 0.5\ 10^{-4}$ s^{-1}, a value close to that quoted above ((*21*) and Table 1). Figure 8a also shows that in the presence of 5 mM MgATP, the concentration of released ^{14}C-TTX 30 min after the cold chase was the same as in the absence of MgATP. All these data show that the presence of TTX on the low affinity site has no effect on the residence time of TTX on the tight site (Figure 8b).

DISCUSSION

Tentoxin Sensitivity of TF_1-ATPase Is Consistent with the Structure of the Putative Inhibitory Tentoxin-Binding Site at the α/β Interface. A first element for understanding the mechanism of TTX inhibition is the structural characterization of the tight binding site. From the sensitivity of different *Nicotiana* species to TTX (*23*) and from directed mutagenesis studies in the alga *Chlamydomonas reinhardtii* (*24*), which is insensitive to TTX, the βAsp83 residue was shown to play a key role in the inhibition of ATP synthesis and hydrolysis by TTX. The presence of an aspartic residue in the β83 position makes the enzyme TTX sensitive, while a glutamic residue at this position makes the enzyme TTX insensitive (*24*). On the other hand, *E. coli* F_1-ATPase is not inhibited

by TTX (*39*), although its β subunit bears an aspartic residue at the corresponding position. Actually, it was recently shown that in the α subunit the sequence containing the residues 127 to 133 (CF_1 numbering) also plays a role in TTX sensitivity (*27*). This sequence is SRLIESP (α127−133) in spinach chloroplasts, TRPIESR (α126−132) in PS3, and FSAVEAI in *E. coli* (α126−132). The first two sequences are highly similar, but not the third. In this report, we have shown for the first time that a non-photosynthetic F_1-ATPase, TF_1, was inhibited by TTX. This observation, and the lack of effect of TTX on MF_1 and EF_1, are consistent with the concomitant roles of βAsp83 and the α127−133 segment in TTX sensitivity. Among MF_1, EF_1, and TF_1, only the latter indeed displays both the suitable β residue (Asp68) and a sequence in α resembling the α127−133 sequence of CF_1. These results are consistent with the fact that TTX binds at an interface between subunits α and β. Using photolabeling (this work), mutagenesis (*23*, *24*), and structural rebuilding data (*28*), together with an early conformational study of TTX (*38*), we identified this site in a cavity belonging to the α subunit, close to the catalytic α/β interface, just under the N-terminal β-barrel domain. The pocket is composed of four conserved aromatic residues that strongly stabilize the TTX molecule (Figure 3). This cavity has its counterpart in MF_1. It contains one glycerol molecule in the recently published (*4*) high-resolution crystallographic structure (*1h8e*, 2 Å resolution) of bovine MF_1. Interestingly, no other glycerol molecule was visible in the crystal. Docking studies showed that interactions occur with α-subunit residues, especially αGlu131, αTyr237, αTyr271, αTyr293, and αArg297 (spinach CF_1 nomenclature). Thus, in the α127−133 segment, thought to play an important role in TTX sensitivity (*27*), αGlu131 is the only residue found to directly interact with the TTX molecule. Intriguingly, this residue is conserved even in TTX-resistant F_1-ATPases. It could however play a key role, and it can be predicted that its mutation could be sufficient to abolish TTX sensitivity. Finally, the MeAla residue of TTX, replaced by a photoactivatable group in the (^{14}C-benzoyl-4-benzoyl)-MeSer^1-TTX molecule, faces the α subunit, which is consistent with our photolabeling experiments.

Asymmetrical Tentoxin Binding Sites in Nucleotide-Free F_1-ATPase. It is important to understand why only one TTX molecule can be tightly bound to F_1, while three potential binding sites exist. One reason could be the different nucleotide occupancies of the three αβ pairs, but it cannot be the only one, because in nucleotide-free TF_1, only one TTX molecule could be bound. Actually, the γ subunit by itself is able to induce an asymmetry of the ATPase subcomplex. It was shown that in nucleotide-free $\alpha_3\beta_3\gamma$ subcomplex reconstituted from CF_1 subunits, but not in $(\alpha\beta)_n$ entities, only one αLys378 residue was accessible, although this amino acid, located at the αβ interface, is remote from the γ subunit (*43*). In addition, binding of the first TTX molecule could diminish the affinity of the other potential binding sites. Filling the first site does influence the other TTX-binding sites, since we have shown that the affinity of the reactivatory site for TTX and analogues was modulated by the toxin bound to the inhibitory site.

Nucleotide Occupancy and Rate of Tentoxin Binding. However, nucleotide occupancy also plays a role in TTX binding, at least in the case of TF_1. With this F_1-ATPase indeed, but not with CF_1-ϵ (*21*), the catalytic turnover dramatically accelerated TTX binding to the inhibitory site. One of the main functional differences between TF_1 and CF_1-ϵ is that purified TF_1 was nucleotide-free, whereas purified CF_1-ϵ contained one ADP molecule tightly bound to a catalytic site (*41*). A possible explanation is that TTX binding to the ADP-loaded αβ pair would be kinetically favored. In the case of CF_1-ϵ, the number of ADP-loaded sites is one in resting state, and remains probably close to one during steady-state ATP hydrolysis, which does not change the probability of an efficient contact between TTX and F_1-ATPase. In the case of TF_1, which is nucleotide-free in resting state, ADP is present on the enzyme only during ATP hydrolysis, which may simply explain the acceleration of TTX-induced inhibition.

In our modeling studies, TTX could not be docked in the ATP-loaded αβ pair, at least in the cavity where it was docked in ADP-loaded and nucleotide-free αβ pairs. The structural reasons for this are not yet clear, because, at first sight, the two nucleotide-loaded αβ pairs do not look very different in this region. Some differences exist in the α270−290 segment, in the vicinity of bound TTX, but at the present time it seems hazardous to ascribe the nucleotide-dependence of TTX binding to these nucleotide-specific changes. It must be emphasized that the TTX binding site is rather constrained and sensitive to the short distance that separates the two α-helices (α233−251 and α290−300) interacting directly with TTX. Docking studies indicate that the site needs to be somewhat distorted to accept the TTX molecule. In such a case, a small initial difference can lead to quite different behaviors when attempts are made to dock a ligand molecule. The most visible nucleotide-dependent changes in the surrounding of the TTX-binding sites is a large movement of the β-barrels located in the N-terminal part of the α subunits, which locks the access to the TTX-binding pocket in the nucleotide-free αβ pair, and lets it open in the two nucleotide-loaded αβ pairs. This conformational change more likely modulates the accessibility of the binding site to external TTX than its ability to retain TTX. Finally, the only αβ pair where TTX could easily reach the site and remain bound would be the ADP-loaded αβ pair. This is consistent with the kinetic preference of TTX for this pair proposed on enzymologic basis.

Mechanism of F_1 Inhibition by Tentoxin. A working model for the mechanism of F_1 inhibition by TTX can be proposed. The catalytic turnover could be blocked by preventing the formation of the energetically unfavorable intermediate having ATP bound on the TTX-bearing αβ pair. This model would also explain an early observation made by Fromme et al. (*18*). When CF_0CF_1 initially bearing tightly bound ADP were submitted to a protonmotive force in the absence of externally added ADP but in the presence of phosphate, a release of ADP and ATP was observed. Tentoxin did not change the total amount of released nucleotides, but ATP release fell to zero and was completely replaced by ADP release. Under this regime of single-site ATP synthesis, this result is easy to explain if one assumes that TTX was initially present on the ADP-loaded site, allowing the release of ADP, but not its transformation into ATP. Fromme et al. (*18*) also found that single-turnover hydrolysis of ATP added at a substoichiometric concentration was not significantly affected by TTX, which is still consistent with our working hypoth-

esis, where ATP molecules cannot bind on the $\alpha\beta$ pair occupied by TTX, and then are readily hydrolyzed on the other sites.

Experiments made on EF_1 have shown that the maximal rate of ATP hydrolysis is reached when the three catalytic sites are occupied (*44*), which suggests that the ternary state of the enzyme with three different nucleotide occupancies used in our modeling studies is not the predominant form encountered during ATP hydrolysis. In accordance with this view, a new crystallographic structure of MF_1 with the three catalytic sites occupied was recently published (*4*). In this model, two catalytic sites are closed and the third one is "half-closed". The existence of these new possible catalytic state of F_1 does not change the fact that during each turn of the γ subunit, the enzyme has to pass three times through the well-established ternary state, with the three $\alpha\beta$ pairs exchanging their roles. As a consequence, forbidding this exchange as suggested above is sufficient for blocking the catalytic cycle, and therefore the proposed mechanism of TTX inhibition remains essentially valid.

The mechanism of CF_1 inhibition by TTX is better explained if one assumes that CF_1 is asymmetrical, even in the absence of added nucleotides. Although the published CF_1 structure is symmetrical (*6*), the authors recognize that this structure may represent an inactive state of the enzyme, and it was suggested that only an asymmetrical structure was competent for tight binding of TTX to CF_1 (*36*).

Mechanism of F_1 Reactivation by Tentoxin Binding on a Low Affinity Site. Whereas the mechanism of F_1 inhibition by TTX at low concentration starts to be roughed out, the mechanism of F_1 reactivation by TTX at high concentration is still mysterious. The number of TTX-binding sites involved in the reactivation process has been also a matter of controversy. Some authors have proposed that the ATPase reactivation induced by binding a second TTX molecule was only partial, and that binding a third TTX molecule was necessary to achieve full reactivation (*22*). In our hands, however, two binding sites were always sufficient to account for the 2-fold action of TTX on CF_1-ϵ (*20*, *21*). The reasons of this discrepancy are not clear. Actually, the only indication for a third TTX-binding site lie in three experimental data points, just initiating a third binding phase, and obtained for TTX concentrations above 2 mM (*22*), close to the limit of TTX solubility in water, which is 4 mM at room temperature (*38*). Moreover, in ref *22*, TTX binding and ATPase inhibition were estimated at different temperatures (respectively, 25 and 37 °C), which makes questionable the correlation between the two processes. As a consequence, although the existence of a third TTX-binding site cannot be fully excluded, only two binding sites were considered in our interpretations. At the present time, there is no direct evidence that these two sites are located on homologous domains of different $\alpha\beta$ pairs, even though it is an attractive hypothesis, as discussed hereafter.

The reactivation process is much more complex than the inhibition one, because it involves a multiplicity of functional ATP-dependent states, discriminated on kinetic basis (*21*). Despite the complexity of the TTX-induced reactivation, some features of its mechanism can be drawn from our present data. Our experiments with TTX analogues, and more especially those with $Lys(Z)^2$-TTX (Figure 4), clearly demonstrate that filling the inhibitory site influences the reactivatory site by modulating its affinity for toxins. The reactivatory loose site could be a binding site that had initially a high potential affinity for TTX, but which was distorted by the presence of the first TTX molecule on the inhibitory site. According to this view, it is reasonable to think that the inhibitory and reactivatory sites are corresponding domains located on two different $\alpha\beta$ pairs.

Once the enzyme is reactivated by two TTX molecules, one may wonder whether the tight and loose sites are interconvertible, and thus whether the TTX occupancy of the two binding sites rotates at the same time as the ATP-loaded, ADP-loaded, and nucleotide-free catalytic sites. If it was the case, TTX initially bound to the high affinity site would become rapidly exchangeable in the presence of TTX at reactivatory concentrations, because the exchange at the loose site is very fast in the presence of ATP (*21*). According to the data of Figure 7, the presence of TTX on the reactivatory site does not accelerate the release of TTX from the inhibitory site. This means that in the enzyme activated with two bound TTX molecules, the conformation of the TTX-binding sites becomes independent of the nucleotide-induced conformational changes of $\alpha\beta$ pairs during catalysis. This unlocks the enzyme, giving rise to a complex even more active than the TTX-free complex in the case of isolated CF_1-ϵ, and only partially reactivated in the case of the CF_0-CF_1 complex (*19*, *42*). In this context, it is important to notice that TTX-activated ATPase certainly retains alternate functioning of the catalytic sites, because proton pumping is preserved in CF_0CF_1 bearing two TTX molecules (*19*, *42*). To conclude, understanding in more detail the very complex and intriguing phenomenon of TTX reactivation remains a challenge. We think that it could bring precious information about mechanical distortions experienced by the ATP synthase subunits during rotational catalysis.

ACKNOWLEDGMENT

We thank Dr. Alain Sanson for critical discussions about docking calculations. We are indebted to Gwénaëlle Moal for having carried out a number of biochemical experiments, including preparation of TF_1. Thanks are due to Geneviève Bouillé for her help in HPLC measurements, and to Véronique Mary for the extraction of CF_1. Beef heart MF_1 was provided by Pr J. Walker (Medical Research Council, Cambridge, United Kingdom). Rat liver mitochondria were provided by Dr. Marc Goubern (Laboratoire de Nutrition et Sécurité Alimentaire, INRA, Jouy-en-Josas, France). Yeast mitochondria were provided by Dr. Jean Velours (Institut de Biochimie et de Génétique Cellulaires, UPR 9026, CNRS-Université de Bordeaux 2, France).

REFERENCES

1. Boyer, P. D. (1997) *Annu. Rev. Biochem. 66*, 717−749.
2. Abrahams, J. P., Leslie, A. G., Lutter, R., and Walker, J. E. (1994) *Nature 370*, 621−628.
3. Bianchet, M. A., Hullihen, J., Pedersen, P. L., and Amzel, L. M. (1998) *Proc. Natl. Acad. Sci. U.S.A. 95*, 11065−11070.
4. Menz, R. I., Walker, J. E., and Leslie, A. G. (2001) *Cell 106*, 331−341.
5. Shirakihara, Y., Leslie, A. G., Abrahams, J. P., Walker, J. E., Ueda, T., Sekimoto, Y., Kambara, M., Saika, K., Kagawa, Y., and Yoshida, M. (1997) *Structure 5*, 825−836.
6. Groth, G., and Pohl, E. (2001) *J. Biol. Chem. 276*, 1345−1352.

7. Stock, D., Leslie, A. G., and Walker, J. E. (1999) *Science 286*, 1700−1705.
8. Seelert, H., Poetsch, A., Dencher, N. A., Engel, A., Stahlberg, H., and Müller, D. J. (2000) *Nature 405*, 418−419.
9. Junge, W., Pänke, O., Cherepanov, D. A., Gumbiowski, K., Müller, M., and Engelbrecht, S. (2001) *FEBS Lett. 504*, 152−160.
10. Noji, H., Yasuda, R., Yoshida, M., and Kinosita, K. (1997) *Nature 386*, 299−302.
11. Pänke, O., Gumbiowski, K., Junge, W., and Engelbrecht, S. (2000) *FEBS Lett. 472*, 34−38.
12. Meyer, W. L., Templeton, G. E., Grable, C. T., Sigel, C. W., Jones, R., Woodhead, S. H., and Sauer, C. (1971) *Tetrahedron Lett. 25*, 2357−2360.
13. Liebermann, B., and Oertel, B. (1983) *Z. Allg. Mikrobiol. 23*, 503−511.
14. Durbin, R. D., and Uchytil, T. F. (1977) *Phytopathology 67*, 602−603.
15. Steele, J. A., Uchytil, T. F., Durbin, R. D., Bhatnagar, P. K., and Rich, D. H. (1976) *Proc. Natl. Acad. Sci. U.S.A. 73*, 2245−2248.
16. Steele, J. A., Durbin, R. D., Uchytil, T. F., and Rich, D. H. (1978) *Biochim. Biophys. Acta 501*, 72−82.
17. Steele, J. A., Uchytil, T. F., and Durbin, R. D. (1978) *Biochim. Biophys. Acta 504*, 136−141.
18. Fromme, P., Dahse, I., and Gräber, P. (1992) *Z. Naturforsch. 47c*, 239−244.
19. Sigalat, C., Pitard, B., and Haraux, F. (1995) *FEBS Lett. 368*, 253−256.
20. Pinet, E., Gomis, J. M., Girault, G., Cavelier, F., Verducci, J., Noel, J. P., and André, F. (1996) *FEBS Lett. 395*, 217−220.
21. Santolini, J., Haraux, F., Sigalat, C., Moal, G., and André, F. (1999) *J. Biol. Chem. 274*, 849−858.
22. Mochimaru, M., and Sakurai, H. (1997) *FEBS Lett. 419*, 23−26.
23. Avni, A., Anderson, J. D., Holland, N., Rochaix, J. D., Gromet-Elhanan, Z., and Edelman, M. (1992) *Science 257*, 1245−1247.
24. Hu, D., Fiedler, H. R., Golan, T., Edelman, M., Strotmann, H., Shavit, N., and Leu, S. (1997) *J. Biol. Chem. 272*, 5457−5463.
25. Tucker, W. C., Du, Z., Hein, R., Richter, M. L., and Gromet-Elhanan, Z. (2000) *J. Biol. Chem. 275*, 906−912.
26. Tucker, W. C., Du, Z., Gromet-Elhanan, Z., and Richter, M. L. (2001) *Eur. J. Biochem. 268*, 2179−2186.
27. Tucker, W. C., Du, Z., Hein, R., Gromet-Elhanan, Z., and Richter, M. L. (2001) *Biochemistry 40*, 7542−7548.
28. Minoletti, C., Santolini, J., Pothier, J., Haraux, F., and André, F. (2002) *Proteins: Struct. Funct. Genet.*, in press.
29. Pezennec, S., Berger, G., Andrianambinintsoa, S., Radziszewski, N., Girault, G., Galmiche, J. M., and Baeuerlein, E. (1995) *Biochim. Biophys. Acta 1231*, 98−110.
30. Berger, G., Girault, G., André, F., and Galmiche, J.-M. (1987*) J. Liq. Chromatogr. 10*, 1507−1517.
31. Bruist, M. F., and Hammes, G. G. (1981) *Biochemistry 20*, 6298−6305.
32. Ohta, S., Tsuboi, M., Oshima, T., Yoshida, M., and Kagawa, Y. (1980) *J. Biochem. (Tokyo) 87*, 1609−1617.
33. Cavelier, F., Enjalbal, C., Santolini, J., Haraux, F., Sigalat, C., Verducci, J., and André, F. (1997) *Lett. Peptide Sci. 4*, 283−288.
34. Santolini, J., Haraux, F., Sigalat, C., Munier, L., and André, F. (1998) *J. Biol. Chem. 273*, 3343−3350.
35. Gomis, J. M., Santolini, J., Cavelier, F., Verducci, J., Pinet, E., André, F., and Noel, J. P. (2000) *J. Labelled Compd. Radiopharm. 43*, 323−330.
36. Gao, F., Lipscomb, B., Wu, I., and Richter, M. L. (1995) *J. Biol. Chem. 270*, 9763−9769.
37. Hausrath, A. C., Grüber, G., Matthews, B. W., and Capaldi, R. A. (1999) *Proc. Natl. Acad. Sci. U.S.A. 96*, 13697−13702.
38. Pinet, E., Neumann, J. M., Dahse, I., Girault, G., and André, F. (1995) *Biopolymers 36*, 135−152.
39. Chen, Z., Spies, A., Hein, R., Zhou, X., Thomas, B. C., Richter, M. L., and Gegenheimer, P. (1995) *J. Biol. Chem. 270*, 17124−17132.
40. Arntzen, C. J. (1972) *Biochim. Biophys. Acta 283*, 539−542.
41. Buy, C., Girault, G., J., and Zimmermann, J.-L. (1996) *Biochemistry 35*, 9880−9891.
42. Pinet, E., Cavelier, F., Verducci, J., Girault, G., Dubart, L., Haraux, F., Sigalat, C., and André, F. (1996) *Biochemistry 35*, 12804−12811.
43. Lowe, K. M., and McCarty, R. E. (1998) *Biochemistry 37*, 2507−2514.
44. Löbau, S., Weber, J., and Senior, A. E. (1998) *Biochemistry 37*, 10846−10853.

BI015938Z